Journal Pre-proofs

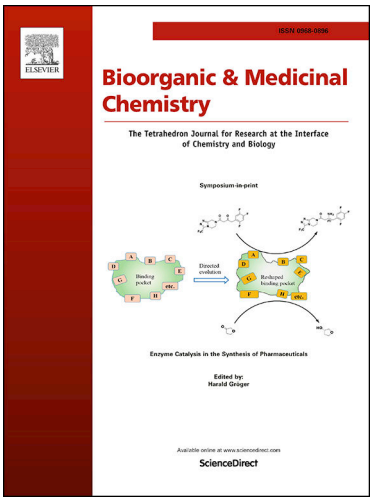

A benzenesulfonamide derivative as a novel PET radioligand for CXCR4

Yoon Hyeun Oum, Dinesh Shetty, Younghyoun Yoon, Zhongxing Liang, Ronald J. Voll, Mark M. Goodman, Hyunsuk Shim

PII: S0968-0896(19)31585-8
DOI: https://doi.org/10.1016/j.bmc.2019.115240
Reference: BMC 115240

To appear in: *Bioorganic & Medicinal Chemistry*

Received Date: 13 September 2019
Revised Date: 20 November 2019
Accepted Date: 25 November 2019

Please cite this article as: Y. Hyeun Oum, D. Shetty, Y. Yoon, Z. Liang, R.J. Voll, M.M. Goodman, H. Shim, A benzenesulfonamide derivative as a novel PET radioligand for CXCR4, *Bioorganic & Medicinal Chemistry* (2019), doi: https://doi.org/10.1016/j.bmc.2019.115240

This is a PDF file of an article that has undergone enhancements after acceptance, such as the addition of a cover page and metadata, and formatting for readability, but it is not yet the definitive version of record. This version will undergo additional copyediting, typesetting and review before it is published in its final form, but we are providing this version to give early visibility of the article. Please note that, during the production process, errors may be discovered which could affect the content, and all legal disclaimers that apply to the journal pertain.

© 2019 Published by Elsevier Ltd.

A benzenesulfonamide derivative as a novel PET radioligand for CXCR4

Yoon Hyeun Oum[a], Dinesh Shetty[b,#1], Younghyoun Yoon[a], Zhongxing Liang[a,c], Ronald J. Voll[b], Mark M. Goodman[b,c], Hyunsuk Shim[a,b,c,*]

[a] Department of Radiation Oncology, [b] Department of Radiology and Image Sciences, Emory University School of Medicine. [c] Winship Cancer Institute, Atlanta, GA 30322.

[#1]Current address: Department of Chemistry, Khalifa University, P. O. Box 127788, Abu Dhabi, United Arab Emirates.

*Corresponding author at: Department of Radiation Oncology, Emory University School of Medicine. 1365 Clifton Road NE, Building C., Atlanta GA, 30322, USA. Email: hshim@emory.edu; Tel: 1-404-712-4564

Journal Pre-proofs

Abstract

CXCR4 is involved in various diseases such as inflammation, tumor growth, and cancer metastasis through the interaction with its natural endogenous ligand, chemokine CXCL12. In an effort to develop imaging probes for CXCR4, we developed a novel small molecule CXCR4-targeted PET agent (compound **5)** by combining our established benzenesulfonamide scaffold with a labeling component by virtue of click chemistry. **5** shows nanomolar affinity (IC_{50} = 6.9 nM) against a known CXCR4 antagonist (TN14003) and inhibits more than 65% chemotaxis at 10 nM *in vitro* assays. Radiofluorinated compound **5** ([^{18}F]**5**) demonstrates a competitive cellular uptake against CXCL12 in a dose-dependent manner. Further, microPET images of [^{18}F]**5** exhibits preferential accumulation of radioactivity in the lesions of λ-carrageenan-induced paw edema, human head and neck cancer orthotopic xenograft, and metastatic lung cancer of each mouse model.

Keywords:

C-X-C chemokine receptor type 4 (CXCR4), CXCL12, molecular imaging probe, positron emission tomography (PET), inflammation, head and neck cancer, metastasis

Highlights

- A novel small molecular CXCR4-targeted PET tracer without chelating moiety is designed based on benzenesulfonamide scaffold *via* chemoinformatic and molecular modeling approach.
- *In vitro* binding assay and chemotaxis inhibition assay affirm the affinity and functional activity of the novel agent with CXCR4.
- The novel CXCR4-targeted F-18 PET agent demonstrates the ability to visualize acute inflammation, head and neck cancer, and cancer lung metastasis in mouse models.

Abbreviations:

GPCRs (G-protein-coupled receptors), CXCR4 (C-X-C chemokine receptor type 4), CXCL12 (C-X-C chemokine ligand 12), SDF-1 (stromal cell-derived factor-1), HIV (human immunodeficiency virus), SCCHN (squamous cell carcinoma of head and neck), PDB (protein databank), EC (effective concentration), DTPA (Diethylenetriamine pentaacetate); DOTA (dodecane tetraacetic acid), NOTA (1,4,7-Triazacyclononane-1,4,7-triacetic acid)

Journal Pre-proofs

1. Introduction

C-X-C chemokine receptor type 4 (CXCR4) is a G-protein-coupled receptor involved in various physiological processes in the hematopoietic and immune systems *via* the interaction with its endogenous partner, chemokine ligand 12 (CXCL12) that is also known as stromal-derived-factor-1 (SDF-1).[1-4] The CXCR4/CXCL12 axis attracts significant notice due to its critical functions in the development of refractory diseases such as HIV infection, metastatic cancer, and autoimmune diseases.[5-10] The pivotal roles of CXCR4 in pathogenesis of such diseases have encouraged an effort to investigate CXCR4-targeted therapeutics.[11-13] Along with this effort, CXCR4-targeted molecules emerge as imaging probes for relevant diseases. For instance, noninvasive imaging of CXCR4 could work as a complementary diagnostic and prognostic biomarker for various metastatic cancers including breast, prostate, lung, colon, and multiple myeloma.[14] Positron emission tomography (PET) is recognized as one of major translational ("bench to bedside") molecular imaging modalities owing to its unparalleled sensitivity and diversity of tracer portfolio to monitor key biological processes of diseases. PET radiotracer can provide early functional data on disease extent, therapy response, identification of recurrence, and stratification of patients for personalized medicine. PET agents require high binding affinity, selectivity, rapid clearance, good tissue penetration, and appropriate metabolism for clear contrast images.

Up to date, various CXCR4-targeted PET radiotracers have been reported.[15] Those PET tracers can be categorized into three classes, based on the nature of targeting groups: i) conjugates of potent peptides such as T140 consisting of 14 amino acids and one disulfide bridge,[16] ii) conjugates of cyclic pentapeptic analogues including FC131,[17] iii) derivatives of nonpeptidic small molecules such as bicyclam AMD3100.[18] A majority of those peptidic PET CXCR4 tracers are the conjugate of metal chelators harnessed to label positron emitting nuclei such as Ga-68 and Cu-64, showing preferential accumulation of radioactivities in the lesions of CXCR4-positive tumors.[19-23] However, the use of large chelators such as DTPA, DOTA, and NOTA often resulted in the reduced ligand affinity due to the steric hindrance upon binding to CXCR4. Moreover, introducing high energy positron emitters such as Ga-68 (β_{max} =1.92 MeV) and Co-55 (β_{max} =1.50 MeV) can lead to the radiolysis of peptides which is hard to suppress, undermining the advantage of chelators that could provide less laborious and time-saving labeling processes. Furthermore, the peptidic agents might have the pharmacokinetic disadvantage such as metabolic instability, low permeability, and in vivo demetallation. Nevertheless, superior affinity of [^{68}Ga]Pentixafor to CXCR4 and favorable pharmacokinetics expedited its clinical translation.[19, 24, 25] However, short half-life ($t_{1/2}$ = 68 min) and low radioproductivity (<1.85 GBq from ^{68}Ge/^{68}Ga generator) of Ga-68 may limit its clinical usage practically,[26] given the radiochemical properties of the current leading PET emitter, F-18 ($t_{1/2}$ = 109 min, radioproductivity > 185 GBq, β_{max} =0.634 MeV). Direct incorporation of F-18 into biomolecules has foundered due to the interfering functionalities in target molecules, harsh reaction conditions, poor regioselectivity, and the low specific activity. Accordingly, labeling peptide with F-18 is usually achieved by

coupling with prosthetic groups, but that also requires time-consuming radiosynthesis, ending up with low radiochemical yield. For example, a couple of nonmetallic, peptidic F-18 PET tracers were reported, but presented with a long labeling time (> $t_{1/2}$) and low radiochemical yield (< 5%).[27, 28]

Recently, nonpeptidic F-18 CXCR4-targeted PET tracers bearing macrocyclic cyclam moiety were reported.[26, 29, 30] In those PET tracers, cyclam moiety was used to label PET emitter, Cu-64, into the established antagonists such as AMD-3100 and AMD-3465.[22, 23, 31, 32] These CXCR4 PET tracers show high T/M ratios (~ 50 for ^{64}Cu-AMD-3100 and ~ 360 for ^{64}Cu-AMD-3465). However, whole-body imaging can be hampered by high liver (36% ID/g) and kidney uptake (38% ID/g) owing to their high lipophilicity.[19] Moreover, the drawbacks of using metal PET emitters still remain as described above. More recently, F-18 labeled AMD-3100 or AMD-3465 were reported by means of prosthetic groups which were linked in the various positions of the antagonists. However, these PET tracers display moderate tumor uptake and significant liver and kidney uptake which is the caveat of the previous CXCR4- PET tracers. Interestingly, the cationic nature of cyclam is hypothesized to contribute to the unwanted liver and kidney uptake along the expression of nonspecific organic cation transporters on the tissues.[30]

The majority of PET agents belongs to small molecules due to their favorable distribution to targets, rapid clearance, and better penetration. At present, most of reported small molecular CXCR4-targeted PET tracers possess chelating moieties such as cyclam, DTPA, NOTA, and DOTA. More importantly, none of the reported tracers has the same structure as their original agents, but rather they are introduced additional chemical moieties for radiolabeling, which may alter the biological properties of the original ligand. For example, an introduction of fluorobenzyl moiety to *c*-terminal of highly CXCR4-specific TN14003 peptide caused the additional affinity to CXCR4-negative red blood cells.[28] In this context, we sought to develop a novel small molecular (< 500 Da) CXCR4-targeted F-18 PET agent not by introducing additional moieties into the established structure of agents for the purpose of labeling, but rather to develop the authentic structure bearing an isotope, fluorine, that can be directly labeled into the molecule by adopting rational drug design approach.

Journal Pre-proofs

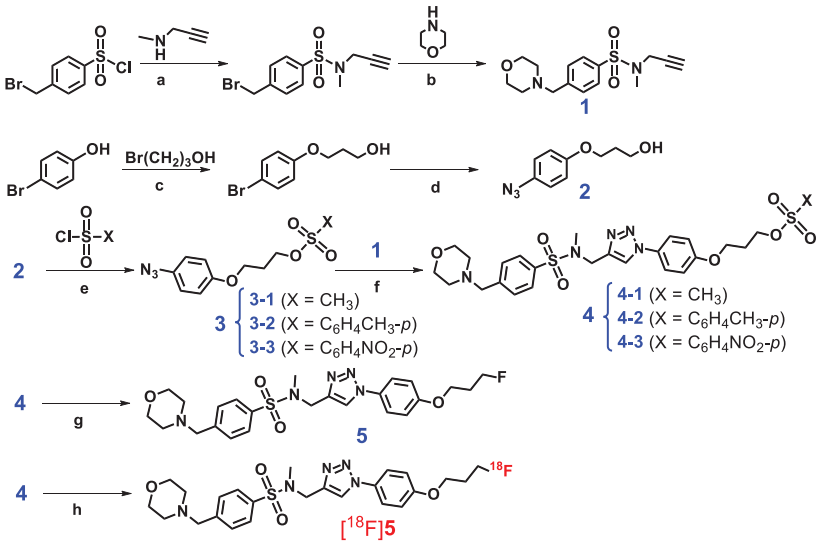

Scheme 1. Reagents and conditions: (a) DCM, TEA, ice bath to r. t., 6 h, 75%; (b) MeCN, r.t., 12 h, 75%; (c) DMF, K_2CO_3, 70 °C, 51%; (d) DMF, NaN_3, CuI, DMEDA, EtOH/H_2O (7:3), 80 °C, 6 h, 80%; (e) DCM, TEA, DMAP, 0 °C, 30 min; 70%, X = CH_3 or $C_6H_4CH_3$-*p* or $C_6H_4NO_2$-*p*; (f) THF/H_2O (10:1), $CuSO_4$, sodium ascorbate, r.t., 3 h, 60%; (g) *t*-BuOH, CsF, reflux, 3 h, 51%; (h) MeCN, K_2CO_3, K_{222}, [^{18}F]F$^-$

2. Materials and methods

1.1. General

All chemical reagents were obtained from commercial sources (Sigma Aldrich Co., St Louis MO, USA) and used without further purification unless otherwise noted. NMR spectra were recorded on a Varian 400 MHz NMR spectrometer or Inova 400 MHz NMR spectrometer. Mass spectra for the small molecules were obtained using an Agilent 1100 LC/MSD VL instrument. Thin Layer Chromatography (TLC) carried out on silica gel 60 (Merck; 230-400 mesh ASTM). RP-HPLC was performed using Beckman Coulter System Gold® on Waters XTerra® Prep C18 Column (10 µm, 10 × 250 mm).

1.2. Cell Culture

Dulbecco's modified Eagle's medium (DMEM) with glutamine, Penicillin/Streptomycin and 0.5% Trypsin-EDTA were purchased from GIBCO (Grand Island, NY). Fetal bovine serum (FBS) was purchased from HyClone (Logan, UT). All cell lines were maintained in 5% CO2 at 37 °C. MDA-MB-231 (human breast adenocarcinoma) cells were cultured in DMEM supplemented with 10% FBS, 100 IU/mL penicillin, 100 µg/mL streptomycin. The human SCC cell line 686LN and its derivatives (nonmetastatic clones 686LN-Ps and metastatic clones 686LN-Ms) were cultured in DMEM/F-12 (Invitrogen) supplemented with 10% FBS, 50 IU/mL penicillin, and 50 µg/mL of streptomycin. Metastatic subclones of E3 cells (CXCR4-positive murine carcinoma) were cultured in DMEM/F-12 (Dulbecco's Modified Eagle Medium/Nutrient Mixture F-12) supplemented with 10% FBS, 50 IU/mL penicillin, 50 µg/mL streptomycin.

1.3. Computational modeling (Molecular Docking)

The default parameters in the Maestro docking module of Schrödinger Suite (v. 9.3) were used unless otherwise noted. The CXCR4 receptors were prepared using the Protein Preparation Wizard in the Schrödinger Suite that assigns bond orders, adds hydrogen atoms, and creates disulfide bonds. The hydrogen-bonding network was optimized at neutral pH 7.0. Receptor grids were constructed with Glide using a 10 × 10 × 10 $Å^3$ boundary box spanning the entire ligand binding pocket and centered on the centroid of either IT1t (from 3ODU, PDB ID) or the Arg2–Nal3 residues of CVX15 (from 3OE0, PDB ID).[33] The designed ligands were prepared using the 2D Sketcher, Lig-Prep, and the OPLS3 force field. Minimized ligand poses were docked flexibly into the CXCR4 receptor grids using Glide Standard Precision (Glide SP) and Extra Precision (Glide XP) and the Epic state-penalties were added to the Glide score. To estimate the binding affinity of designed ligands to CXCR4, the energy of ligand-receptor complex (MMGBSA dG Bind) was calculated using Prime MM-GBSA method and compared to the values of known active CXCR4-ligands.

1.4. Chemical Synthesis

Synthesis of Compound 1. To a solution of 4-(bromomethyl)benzene-1-sulfonyl chloride (1.00 g, 3.71 mmole) in DCM was added N-methylpropargylamine (0.28 g, 4.08 mmole, 1.1 eqv.) under cooling. The reaction mixture was stirred at 0 °C for 6 h and monitored by TLC. After completion of the reaction, the mixture was purified by flash column chromatography, eluting with ethyl acetate/hexane (1:3, *v/v*). ^{1}H NMR (400MHz, CD_3Cl): δ 7.80 (2H, m), 7.55 (2H, m), 4.51 (2H, s), 4.05 (2H, d, J_{13} = 2.4 MHz), 2.86 (3H, s), 2.06 (1H, t, J_{13} = 2.4 MHz) ppm. The purified compound was obtained as white crystalline powder (835 mg, yield 75%) and dissolved in acetonitrile, then was added morpholine (267 mg, 1.1 eqv.). The reaction mixture was stirred at room temperature overnight. After the completion of the reaction, the mixture was filtered through celite and organic solvent was removed by rotary evaporation. The residue was dissolved in DCM and washed with water, brine, and dried over $MgSO_4$ and concentrated. The crude product was purified by flash column chromatography, eluting with DCM/methanol (10:3, *v/v*). The purified compound was obtained as a white powder. (724 mg, yield 85%). ^{1}H NMR (400MHz, CD_3Cl): δ 7.80 (2H, m), 7.60 (2H, m), 4.05 (2H, d, J_{13} = 2.4 MHz), 3.82 (4H, m), 3.73 (2H, s), 2.85 (3H, s), 2.62 (4H, m), 2.07 (1H, t, J_{13} = 2.4 MHz) ppm.

Synthesis of Compound 2. Compound **2** was synthesized as described previously.[34] Briefly, to a suspension of 4-bromophenol (5.00 g, 28.90 mmol) and K_2CO_3 (5.99 g, 43.35 mmol) in DMF (100 mL) was added 3-bromo-1-propanol (6.02g, 43.35 mmol), and the reaction mixture was heated to 70 °C. After 12 h, the reaction mixture was cooled to room temperature, quenched with water and aqueous NH_4Cl. The organic compound was extracted with ethyl acetate (3 × 100 mL). The combined organic layer was washed with brine (3 × 100 mL), dried over $MgSO_4$, and then concentrated under reduced pressure. The residue was purified by flash column

chromatography, eluting with ethyl acetate/hexane (1:4, *v/v*) to afford 3-(4-bromophenoxy)propan-1-ol as a white solid (3.4 g, yield 51%). ^{1}H NMR (400MHz, CD3Cl): δ 7.35 (2H, d), 6.76 (2H, d), 4.04 (2H, t), 3.81 (2H, t), 2.24 (1H, br), 2.06~1.94 (2H, m) ppm. The 3-(4-bromophenoxy)propan-1-ol (1.00 g, 4.33 mmol), sodium azide (563 mg, 8.66 mmol), sodium ascorbate (44 mg, 0.22 mmol), copper iodide (82 mg, 0.43 mmol), and *N*, *N*'-dimethylethylenediamine (DMEDA, 70 μL, 0.65 mmol) were placed in a two-necked round bottom flask equipped with a reflux condenser, and 13 mL of ethanol/water (7:3, *v/v*) was added under N_2 atmosphere. The reaction mixture was stirred at 80 °C for 6 h, and then cooled down to room temperature, quenched with water, and organic compounds were extracted with ethyl acetate (3 × 100 mL). The combined organic layer was washed with brine (3 × 100 mL), dried over $MgSO_4$ and concentrated under reduced pressure. The residue was purified by flash column chromatography, eluting with ethyl acetate/hexane (2:3, *v/v*) to afford compound **2** as yellow oil (669 mg, 80% yield). ^{1}H NMR (400MHz, CD_3Cl): δ 6.95~6.84 (4H, m), 4.06 (2H, t), 3.82 (2H, t), 2.35 (1H, br), 2.07~1.95 (2H, m) ppm.

Synthesis of Compound 3. (compound **3-1**: X = CH_3 or **3-2**: $C_6H_4CH_3$-*p* or **3-3**: $C_6H_4NO_2$-*p*). To a solution of 3-(4-azidophenoxy)-propan-1-ol (498 mg, 2.58 mmol) and trimethylamine (432 μL, 3.09 mmol) in DCM (10 mL) was added slowly methanesulfonyl chloride for **3-1** or toluenesulfonyl chloride for **3-2** or 4-nitrobenzenesulfonyl chloride for **3-3** (1.2 eqv.) in DCM at 0 °C over 10 min. After 30 min, the reaction was quenched with water and aqueous NH_4Cl, and organic compound was extracted with DCM (3 × 100 mL). The combined organic layer was dried over $MgSO_4$ and then concentrated under reduced pressure. The residue was purified by flash column chromatography, eluting with ethyl acetate/hexane (1:4, v/v) to afford 3-(4-azidophenoxy) propyl methanesulfonate (**3-1**, white solid, yield 64%). ^{1}H NMR (400MHz, CD_3Cl): δ 6.95~6.84 (4H, m), 4.42 (2H, t), 4.06 (2H, t), 2.98 (3H, s), 2.20 (2H, dd) ppm; 3-2: 3-(4-azidophenoxy) propyl toluenesulfonate (**3-2,** white solid, yield 70%). ^{1}H NMR (400MHz, CD_3Cl): δ 7.75 (2H, m), 7.25 (2H, m), 6.90 (2H, m), 6.72 (2H, m), 4.23 (2H, t), 3.90 (2H, t), 2.37 (3H, s), 2.09 (2H, dd) ppm; 3-(4-azidophenoxy) propyl nitrobenzenesulfonate (**3-3**, yellow solid, yield 79%). ^{1}H NMR (400MHz, CD_3Cl): δ 8.23~8.20 (2H, m), 8.03~8.01 (2H, m), 6.88~6.85 (2H, m), 6.67~6.64 (2H, m), 4.43 (2H, t), 3.86 (2H, t), 2.13 (2H, dd).

Synthesis of Compound 4. (compound **4-1**: X = CH_3 or **4-2**: $C_6H_4CH_3$-*p* or **4-3**: $C_6H_4NO_2$-*p*). To a mixture of compound **1** (50 mg, 0.162 mmol) and **3-1** or **3-2** or **3-3** (1.1 eqv.) in THF 2 mL was added aqueous solution of 1 M $CuSO_4$ 100 μL and 1 M sodium ascorbate 100 μL. The mixture was stirred at room temperature for 3 h. The reaction mixture was extracted with ethyl acetate (3 × 50 mL) and dried over $MgSO_4$, and then concentrated under reduced pressure. The residue was purified by flash column chromatography, eluting with DCM/methanol (10:1, v/v) to afford compound **4-1** (X = CH_3) (white solid, yield 61%). ^{1}H NMR (400MHz, DMSO-d6): δ 8.59 (1H, s), 7.76~7.73 (4H, m), 7.50 (2H, d), 7.15 (2H, d), 4.38~4.36 (4H, m), 4.15 (2H, t), 3.54 (4H, m), 3.53 (2H, s), 3.34 (6H, m), 3.20 (3H, s), 2.75 (3H, s), 2.30 (4H, m), 2.16 (2H, m) ppm.

^{13}C NMR (400MHz, DMSO-d6): δ 158.3, 143.4, 142.1, 135.8, 129.8, 127.8, 122.1, 115.9, 88.6, 66.7, 64.3, 62.0, 58.2, 53.5, 44.7, 36.9, 35.4, 29.2 ppm. HRMS (ESI-TOF) m/z: $[M+H]^+$ Calcd for $C_{25}H_{34}N_5O_7S_2$ 580.18; Found 580.19. Anal. Calcd for $C_{25}H_{33}N_5O_7S_2$: C, 51.80; H, 5.74; N, 12.08; S, 11.06; F, 3. Found: C, 51.64; H, 5.67; N, 11.99; S, 10.91 or compound **4-2** (X = $C_6H_4CH_3$-*p*) (white solid, yield 71%) ^{1}H NMR (400MHz, DMSO-d6): δ 8.60 (1H, s), 7.51 (2H, d), 7.39 (2H, d), 7.00 (2H, d), 4.36 (2H, s), 4.20 (2H, t), 3.98 (2H, t), 3.54 (4H, m), 3.50 (2H, s), 2.75 (3H, s), 2.33~2.30 (6H, m), 2.95 (2H, m) ppm. ^{13}C NMR (400MHz, DMSO-d6): δ 158.6, 145.3, 144.0, 142.8, 135.4, 130.6, 130.4, 129.8, 128.0, 127.8, 125.8, 122.6, 122.0, 115.1, 68.0, 66.6, 64.0, 62.0, 53.5, 45.3, 35.4, 28.5, 21.5 ppm. HRMS (ESI-TOF) m/z: $[M+H]^+$ Calcd for $C_{31}H_{38}N_5O_7S_2$ 656.21; Found 656.22. Anal. Calcd for $C_{31}H_{37}N_5O_7S_2$: C, 56.78; H, 5.69; N, 10.68; S, 9.78. Found: C, 56.48; H, 5.59; N, 10.48; S, 9.80. or compound **4-3** (X = $C_6H_4NO_2$-*p*) (yellow solid, yield 74%) ^{1}H NMR (400MHz, DMSO-d6): δ 8.57 (1H, s), 8.31 (2H, d), 8.17 (2H, d), 7.75 (2H, d), 7.68 (2H, d), 7.51 (2H, d), 6.95 (2H, d), 4.36~4.34 (4H, m), 3.95 (2H, t), 3.54~3.51(6H, m), 2.75 (3H, s), 2.31 (3H, br), 2.10 (2H, m) ppm. ^{13}C NMR (400MHz, DMSO-d6): δ 158.0, 150.4, 142.3, 140.0, 135.6, 130.0, 129.3, 127.3, 126.9, 124.9, 123.0, 122.1, 121.3, 115.1, 68.8, 66.1, 63.2, 61.6, 53.1, 44.9, 35.0, 27.9 ppm. HRMS (ESI-TOF) m/z: $[M+H]^+$ Calcd for $C_{30}H_{35}N_6O_9S_2$ 687.18; Found 687.19. Anal. Calcd for $C_{30}H_{34}N_6O_9S_2$: C, 52.47; H, 4.99; N, 12.24; S, 9.34. Found: C, 52.17; H, 5.00; N, 12.00; S, 9.41.

Synthesis of Compound 5. To a solution of compound **4-1** (100 mg, 0.173 mmol) in *tert*-butanol (2 mL) was added Cesium fluoride (131 mg, 5.0 eqv.) and refluxed the reaction mixture for 3 h. After the completion of the reaction, the reaction solvent was removed by rotary evaporation. The residue was dissolved in DCM and washed with water, brine, and dried over $MgSO_4$ and concentrated. The crude product was purified by flash column chromatography, eluting with DCM/methanol (10:1, v/v). The purified compound was obtained as a white powder. (44 mg, yield 51%). ^{1}H NMR (400MHz, DMSO-d6): δ 8.59 (1H, s), 7.76~7.72 (4H, m), 7.49 (2H, d), 7.14 (2H, d), 4.69 (1H, t), 4.57 (1H, t), 4.36 (2H, s), 4.15 (2H, t), 3.53 (4H, br), 3.49 (2H, s), 2.75 (3H, s), 2.30 (4H, br), 2.14 (2H, m) ppm. ^{13}C NMR (400MHz, DMSO-d6): δ 158.4, 143.5, 142.3, 135.4, 130.0, 129.3, 127.3, 122.2, 212.6, 115.4, 80.8 ($^1J_{C\text{-}F}$ = 643 Hz), 66.1, 64.0 ($^3J_{C\text{-}F}$ = 2.4 Hz), 61.6, 53.1, 44.9, 35.0, 29.6 ($^2J_{C\text{-}F}$ = 26 Hz) ppm. ^{19}F NMR (300MHz, CD_3Cl): δ 7.53 (1F, m). HRMS (ESI-TOF) m/z: $[M+H]^+$ Calcd for $C_{24}H_{31}FN_5O_4S$ 504.20; Found 504.21. Anal. Calcd for $C_{24}H_{30}FN_5O_4S$: C, 57.24; H, 6.00; N, 13.91; S, 6.37; F, 3.77. Found: C, 57.07; H, 5.88; N, 13.99; S, 6.46; F, 3.67.

*1.5. Radiosynthesis (Synthesis of Compound [^{18}F]**5**)*

No-carrier-added $[^{18}F]F^-$ was obtained through the nuclear reaction $^{18}O(p, n)^{18}F$ by irradiation of ^{18}O-enriched water. After the delivery of $[^{18}F]F^-$ from the cyclotron, the radioactivity was passed through an anion exchange resin cartridge to trap $[^{18}F]F^-$. $[^{18}F]F^-$ was then eluted with a potassium carbonate solution into a vessel containing Kryptofix 2,2,2 (K_{222}) and the mixture was dried by azeotropic distillation with acetonitrile. Compound **4** (**4-1** or **4-2** or **4-3**) in anhydrous acetonitrile was added to the dried $K_{222}/K[^{18}F]F^-$ and the mixture was heated at 120 ˚C for 30

min to produce [^{18}F]compound **5**. The crude reaction mixture was purified by HPLC (Prep column, methanol/water = 1/1), then the collected fraction including [^{18}F]**5** was trapped on C18 solid phase extraction cartridge and eluted by ethanol into a vial containing isotonic saline. A total 123 mCi of [^{18}F]**5** was obtained from 1389 mCi of [^{18}F]$^{-}$ fluoride in a synthesis time of approximately 100 min. The precursors (**4-1, 4-2**, and **4-3**) provided 16.5 % (from **4-1**), 15.7% (from **4-2**), and 27.0% (from **4-3**) decay corrected yield (DCY) of [^{18}F]**5** respectively (Fig. S6A using **4-1**). We were able to obtain [^{18}F]**5** from 3 different precursors (**4-1, 4-2**, and **4-3**). Because the mesyl precursor provided the highest radiochemical yield, we only showed the chromatogram of the mesyl precursor. For the chromatogram of standard cold compound **5**, we included in Fig S6. C at the bottom. Because low Signal of [^{18}F]**5** in crude mixture in HPLC, we used the chromatogram of [^{18}F]**5** in the dose to confirm the radiotracer identity by co-injecting standard cold compound **5**. Since the specific activity of [^{18}F]**5** was not directly determined due to the detection limit of UV detector in HPLC, we assume that the maximum amount of nonradioactive material in the final dose arising from the precursor is about 1μg. On the basis of an HPLC serial dilution injection of the aqueous solution of cold compound **5** (100μg/mL, 10μg/mL, 1μg/mL, 0.1μg/mL, and 0.01μg/mL; starting from 0.1μg/mL, no UV peak corresponding to **5** was observed on HPLC chromatogram) using the same analytical HPLC labeling method and a 123 mCi yield in 7.5 mL solution at end of synthesis, the amount of unlabeled material in the final product would not exceed 0.06 μg/mCi. Quality control HPLC of the labeled [^{18}F]**5** showed chemical and radiochemical purity > 99%. The saline solution of [^{18}F]**5** was sterilized by filtration through a 0.2-micron filter for further study. The cold (radio-inactive) standard cold compound **5** was co-injected with dose and HPLC traces displayed the same elution time which supported that the dose was the desired hot compound ([^{18}F]**5**) (Fig. S6C).

1.6. In vitro affinity assay

MDA-MB-231 cells were cultured in an eight-well slide chamber for two days. The cells were pre-incubated with the antagonist (compound **5** or AMD-3100) for 15 min, and then fixed with 4% formaldehyde. The fixed cells were subsequently incubated for 45 min with biotinylated-TN14003 (CXCR4-specific antagonist peptide). Then, cells were incubated for 30 min in streptavidin–rhodamine red-x at a 1:150 dilution (Jackson Immuno Research Laboratories, West Grove, PA, USA) after washing three times with PBS. The slides were washed with PBS and mounted in an anti-fade mounting solution (Molecular Probes, Eugene, OR, USA). The pictures of stained cells for each treatment were taken on a Nikon Eclipse E800 microscope. Pictures were analyzed quantitatively with ImageJ. The inhibition % of the antagonist (compound **5** or AMD-3100) was tested at 0.01, 0.1, 1, 10, 100, 1000, and 10000 nM and IC_{50} value for the antagonist (compound **5** or AMD-3100) was fitted with GraphPad Prism 4.

1.7. In vitro Matrigel invasion assay

Matrigel invasion chambers from BD Biocoat Cellware (San Jose, CA, USA) were used for invasion assays. MDA-MB-231 cells were cultured on a layer of Matrigel in the upper chamber

with the antagonist (compound **5** or AMD-3100) at 1, 10, 100, and 1000 nM, while 200 ng/ml of CXCL12 was added in the lower chamber as a chemoattractant. The Matrigel invasion chamber was incubated for 22 h in a humidified tissue culture incubator. After noninvading cells were removed from the top of the Matrigel with a cotton-tipped swab. Invading cells at the bottom of the Matrigel were fixed in methanol and stained with H&E. The invasion rate was determined by counting the H&E-stained cells.

*1.8. In vitro competition binding assay with hot compound **5***

CXCR4-positive metastatic squamous cell carcinoma of head and neck (SCCHN) cells were preincubated with radiolabeled ligand suspension in binding buffer (BB, 1 mg/mL BSA in PBS, 180 μL of cell suspension of 1×10^7 cells/mL + 5 μL solution of [^{18}F]compound **5** (1 μCi/μL) in each tube for 15 min, and 20 μL of natural ligand (CXCL12) solutions were added to make up final concentrations of 11, 33, and 100 nM, and then incubated for 60 min with gentle vortexing every 10 min. The tubes were centrifuged, and the supernatant was removed, then the cells were washed with 0.5 mL cold BB twice. 200 μL of cold BB was added to each tube and 50 μL of cell suspension was taken from each tube (triplicate). Finally, radioactivity of each tube was measured by a gamma counter.

*1.9. In vivo μPET/CT study for inflammation model with hot compound **5***

Acute inflammation was induced by subcutaneous injection of 50 μL of λ-carrageenan (1% w/v in saline) into one of the hind paws of male nude mice (6 weeks, 20 g, Jackson Laboratory, Strain JAZ 007850 J:NU). An apparent edema response was observed 5 h after the λ-carrageenan injection. 150 μCi of radiotracer ([^{18}F]compound **5**) in 150 μL PBS was injected to mice through the tail vein (i.v.). Then, mice were anaesthetized with isoflurane (1.0 ~ 2.0%) and 90 min after injection of radiotracer, PET images were acquired for 20 min using an Inveon micro PET/CT Preclinical Scanner (Siemens). Subsequent CT images were acquired for 10 min.

*2.10. In vivo μPET/CT study for head and neck cancer with hot compound **5***

SCCHN (squamous cell carcinoma of head and neck) tumor cells were inoculated (2.5×10^6 cells in 50 μL) to female nude mouse (6 weeks, ~20 g, Harlan Sprague Dawley, Strain: HSD : Athymic Nude-Foxn1<nu>) in the area of neck (orthotopic), 3 weeks before in vivo test. PET/CT images were acquired using the same protocol as the paw edema case.

*2.11. In vivo μPET/CT study with cold compound **5** (Blocking study)*

Before in vivo blocking assay, toxicity of cold compound **5** was tested. 10 mg/kg dose (vehicle: 10% DMSO + 90% PBS including 45% cyclodextrin) of compound **5** was injected to the mouse (female, 6 weeks, 20g, Jackson Laboratory, JAX000819 B6 Cg-Foxnl <nu>/J.) through the tail vein (i.v.), which showed no toxicity to mice. For the blocking, 200 μL of cold compound **5** solution (30 mg/kg, 10% DMSO, 90% PBS including 45% cyclodextrin) was administered to the mouse (i.p.) (male, 6 weeks, 20 g, Jackson Laboratory, Strain JAZ 007850 J:NU) 30 min prior to

[^{18}F]**5** injection (i.v.). PET/CT images were acquired using the same protocol as the paw edema case.

*2.12. In vivo μPET/CT study for mouse lung metastasis model with hot compound **5***

Six-week-old female nude mice (Harlan Sprague Dawley, Strain: HSD : Athymic Nude-Foxn1<nu>) were given injections of 2.0 × 10^6 metastatic subclones of E3 (CXCR4-positive murine carcinoma cells donated by Dr. Zhuo (Georgia) Chen[35]) through the tail vein. After 8 weeks, PET/CT images were acquired using the same protocol as the paw edema case.

3. Results

3.1. Design and Synthesis of Small Molecule CXCR4 F-18 PET Ligand

Using the benzenesulfonamide scaffold of CXCR4 antagonist which was reported previously,[36] we designed novel molecular structures containing a fluorine atom to synthesize CXCR4-targeted F-18 PET agents. First, we analyzed a series of the reported benzenesulfonamide compounds by chemoinformatics model (fingerprint-based KPLS in Canvas, Schrödinger Suite) to access each atom's contribution to biological activities such as binding affinity and chemotaxis inhibition. (Fig. S1). The analysis indicated each atom's positive or negative contribution to the binding affinities of compounds. Thus, we replaced the negatively contributing moiety with fluorine-containing group to label the compound with F-18

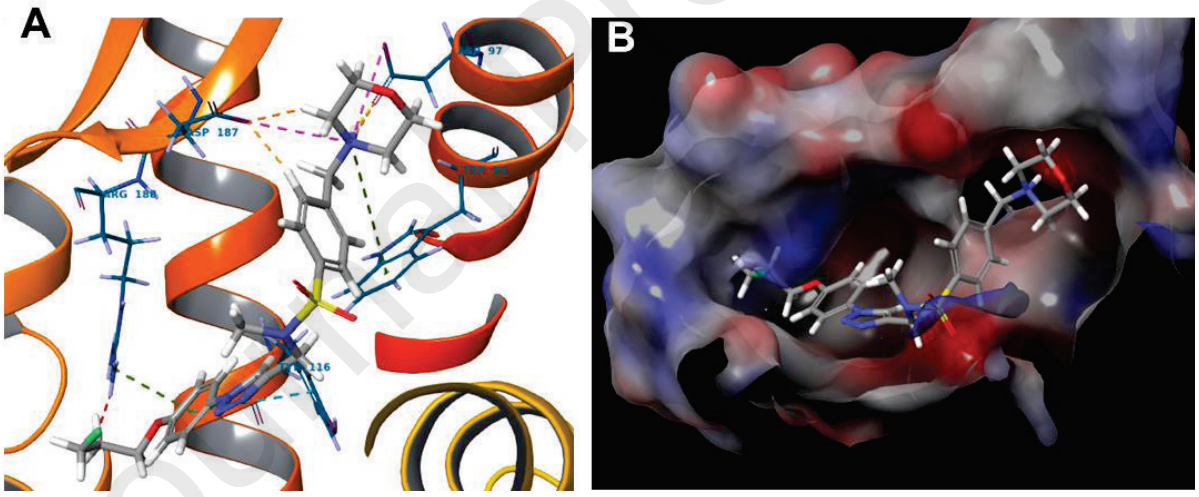

Figure 1. Docking pose of Compound 5 in the CXCR4 crystal structure (A) Docking pose representing the interactions of compound **5** with the critical residues of CXCR4 (W94, D97, Y116, D187, R188). Dotted lines show putative hydrogen bonds. (B) Molecular surface representation of the binding pocket of CXCR4 receptor in the crystal structure [PDB ID: 3OE0] colored by atom type (carbon and hydrogen: light grey; nitrogen: blue; oxygen: red). The ligand (Compound **5**) is represented by stick models.

radionuclide without losing the affinity. Next, we estimated the binding affinity of the designed compounds through molecular docking model using Glide (Schrödinger Suite). In order to validate our docking model first, we conducted "redocking" experiment (Fig. S2) and examined the correlation between MM-GBSA dG binding energies and in vitro affinity data (IC_{50}) ($r^2 \approx 0.7$). Then, we compared the calculated binding energy of designed compounds with the values

of known benzenesulfonamide antagonists. We chose the best structure (compound **5**) which showed competitively high binding energy (-63.7 kcal/mole) and reasonable pose representing the interactions with the critical residues (W94, D97, Y116, D187, R188)[37] of CXCR4 which were reported previously (Fig. 1, Fig. S3). To synthesize the best compound, we prepared compound **1** and **3** respectively as described in the previous literatures[34, 36, 38] (Scheme 1). Then, we introduced 3 different leaving groups (mesyl, tosyl, and nosyl) into the precursor of compound **5** to increase labeling yield and purify the labeled compound from the unlabeled compounds more effectively. Then, we adopted copper-catalyzed azide-alkyne cycloaddition (CUAAC, click chemistry) which allows an easy and straightforward synthetic route for the precursors (compound **4**) of the F-18 PET ligand ([^{18}F]compound **5**). To optimize radiochemical synthesis, we prepared [^{18}F]**5** from the corresponding 3 different precursors (mesyl, tosyl, and nosyl). Nosyl precursor provided the best radiochemical yield, but mesyl precursor showed the best separation of leveled compound from unlabeled impurities as the HPLC profile indicates (Fig. S6). We also prepared F-19 cold compound **5** as a standard for purification and to test its biological activities before in vivo PET evaluation of hot compound [^{18}F]**5**.

3.2. In vitro affinity and chemotaxis inhibition assays

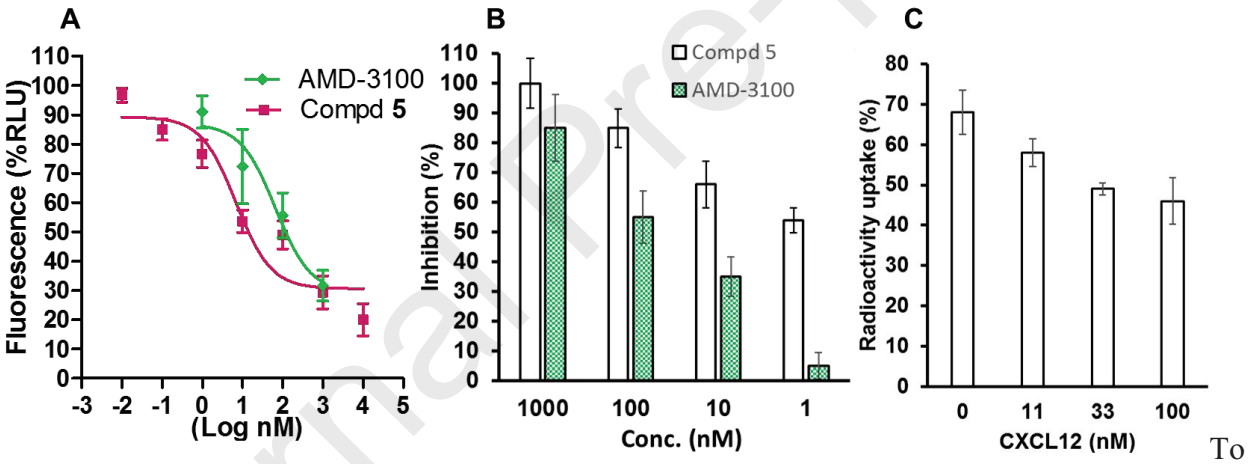

Figure 2. **In vitro assays of compound 5** (A) Binding assay using the biotinylated CXCR4 antagonist TN14003. MDA-MB-231 cells on an 8-well slide chamber were treated with various concentrations of the antagonist (compound **5** or AMD-3100) and biotin-labeled TN14003. After washing, cells were incubated with streptavidin-rhodamine. Mean fluorescence intensity was quantitated with ImageJ. IC_{50} (compd 5) = 6.9 nM; IC_{50} (AMD-3100) = 66 nM. (B) Matrigel invasion assay induced by CXCR4/CXCL12-mediated chemotaxis using MDA-MB-231 cells in the presence of the antagonist (compound **5** or AMD-3100). The invasion % was determined by counting the H&E-stained cells. (C) In vitro celluar uptake assay with hot compound [^{18}F]**5** and CXCL12 as a competitive ligand. CXCR4-positive metastatic squamous cell carcinoma of head and neck (SCCHN) cells were preincubated with radiolabeled ligand and natural ligand (CXCL12) were added to make final concentrations of 11, 33, and 100 nM. After 60 min incubation and washing, radioactivity of each tube was measured by a gamma counter (triplicate). Error bars indicate standard deviations.

To test the affinity of the designed PET ligand, we performed *in vitro* binding assay as described previously,[39] which showed 6.9 nanomolar IC_{50} of compound **5** to block CXCR4-specific antagonist peptide, TN14003. As a positive control, we also tested an established CXCR4 antagonist, ADM-3100, which showed IC_{50} (66 nM) close to reported values. (Fig. 2A, Fig.

S4). As a secondary functional assay, we employed Matrigel invasion assay[39] to test the antagonistic activity of compound **5** against CXCR4/CXCL12 axis. Chemokine CXCL12 (or SDF-1) is the natural ligand of CXCR4 and strongly chemotactic for the CXCR4 positive cells. Compound **5** inhibited 85% of chemotactic invasions at 100 nM in the Matrigel assay, which is better than AMD-3100 (55%) (Fig. 2B, Fig. S5).

3.3. In vitro cellular uptake assays

To determine whether compound **5** binds to the same target (CXCR4) as endogenous chemokine ligand (CXCL12), we performed in vitro competition binding assays with radioactive [^{18}F]**5** and CXCL12. At first, CXCR4-positive cells (686LN) were labeled with [^{18}F]**5** showed strong radioactivity due to the retention of [^{18}F]**5** in the absence of CXCL12. Then, as we increase the concentration of CXCL12, the observed radio activity is reduced by 32.4±8.5% (100 nM), 27.9±2.2% (33 nM), 14.7±5.1% (11 nM) in a dose-dependent manner. This result suggests that [^{18}F]**5** competes for the same binding sites of endogenous ligand, CXCL12 (Fig. 2C).

3.4. In vivo imaging study

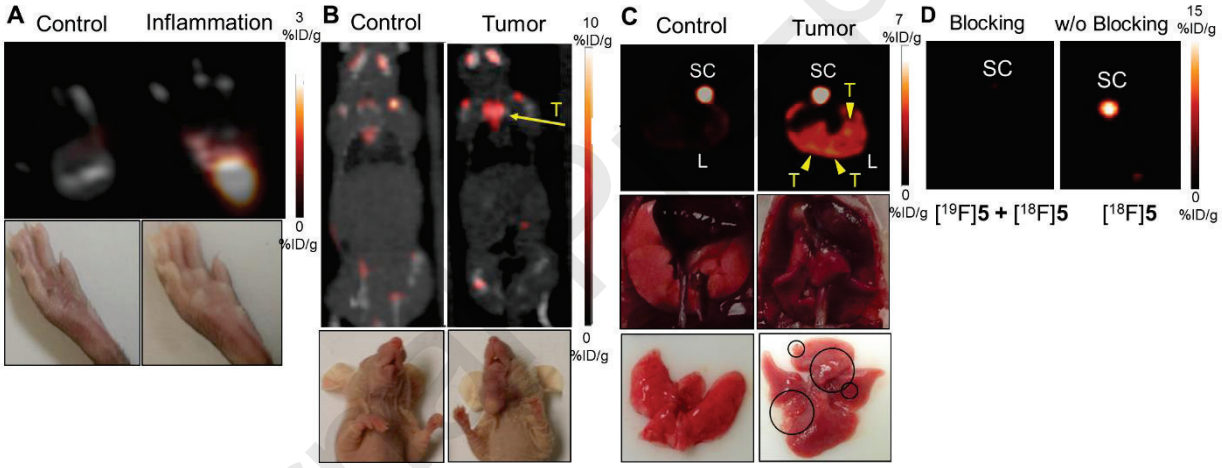

Figure 3. µPET/CT images of [^{18}F]5 (A) Acute inflammation was induced by subcutaneous injection of λ-carrageenan into one of the hind paws of male nude mice. An apparent edema response was observed 5 h after the λ-carrageenan injection. Radiotracer ([^{18}F]**5**) was injected to mice through the tail vein. Then, mice were anaesthetized with isoflurane. 90 min after injection of radiotracer, PET images were acquired for 20 min using an Inveon micro PET/CT Preclinical Scanner (Siemens). Subsequent CT images were acquired for 10 min. (B) SCCHN (squamous cell carcinoma of head and neck) CXCR4-positive tumor cells were inoculated (2.5×10^6 cells in 50 µL) to female nude mouse in the area of neck (orthotopic), 3 weeks before in vivo test. PET/CT images were acquired using the same protocol as the paw edema case. Tumor is indicated by yellow arrows. (C) Six-week-old female nude mice were given injections of 2.0×10^6 metastatic subclones of E3 (CXCR4-positive murine carcinoma cell line) through the tail vein. After 8 weeks, PET/CT images were acquired using the same protocol as the SCCHN cancer study. Representative [^{18}F]**5** transverse PET images of 90 min p.i., Yellow arrows and text denote the location of the tumor (T), lung (L), spinal column (SC). The circles in the bottom figure indicate induced metastatic tumor nodules. (D) µPET transverse plane images with cold + hot (Blocking, left) compd. vs only hot compd. (right); For the blocking, 200 µL of cold [^{19}F]**5** solution (30 mg/kg, 10% DMSO, 90% PBS including 45% cyclodextrin) was administered to the mouse (i.p.) (male, 6 weeks, 20 g, Jackson Laboratory, Strain JAZ 007850 J:NU) 30 min prior to [^{18}F]**5** injection (i.v.). PET images were acquired using the same protocol as the paw edema case. This experiment suggests the specificity of compound **5** to bind CXCR4-positive stem cells in bone marrow.

After testing the affinity and antagonistic activity of compound **5**, we are encouraged to conduct in vivo imaging studies using animal models. CXCR4/CXCL12 interaction has been reported to play an important role in the recruitment of immune cells during early phase of inflammation.[39-43] Therefore, we tested the ability of compound [^{18}F]**5** to visualize λ-carrageenan-induced inflammation in a mouse model as described above, which showed significantly higher radioactivity in the lesion of paw edema (Fig. 3A). Mean tracer uptake, as determined by injected dose per gram (%ID/g), was found to be statistically different, using a paired Student's t test (p = 0.0015, n =5), between paw edema (1.53 ± 0.08 %ID/g) and negative control. Then, to test the ability to visualize tumor non-invasively, we evaluated the accumulation of [^{18}F]**5** in xenograft SCCHN expressing CXCR4 in orthotopic mouse model. After administration of [^{18}F]**5**, mice exhibited preferential accumulation in sites of tumor growth (4.00 ± 0.28 %ID/g), relative to muscle (p = 0.005, n=5), in our orthotopic xenograft model (Fig. 3B). Further, we evaluated the ability of [^{18}F]**5** to image metastatic tumors arising in the lung using athymic nude mouse model as described above. After administration, [^{18}F]**5** displayed preferential accumulation in lung metastatic tumors (1.66 ± 0.14 %ID/g). Based on Standardized Uptake Value (%ID/g), a tumor-to-lung ratio of 3:1 (p = 0.002, n = 5) was achieved by conclusion of the 90-min scan (Fig. 3C).

Table 1. Biodistribution of [^{18}F]**5** at 90 min

Organ	SUV (%ID/g)	P (n = 5)
Paw edema	1.53 ± 0.08	0.002
SCCHN tumor	4.00 ± 0.28	0.005
Metastatic tumor in lung	1.66 ± 0.14	0.002
Lung	0.50 ± 0.04	n/a
Liver	1.20 ± 0.12	n/a
Kidney	3.22 ± 0.60	n/a
Muscle	0.16 ± 0.03	n/a
Heart	0.54 ± 0.08	n/a
Spleen	0.58 ± 0.07	n/a
Small intestine	0.68 ± 0.04	n/a
Large intestine	0.17 ± 0.04	n/a

Of note, we found illuminated bone marrow presumably due to the enrichment of non-neoplastic CXCR4-positive stem cells (not from defluorination and uptake in the bone). To test our hypothesis, we performed a blocking experiment with cold compound **5** (F-19 compound **5**). After administering of cold compound **5**, we observed significant decreased (95% >) radioactivity in the bone regions of the blocking models, which suggests specific binding of compound **5** to CXCR4-positive stem cells in bone marrow (Fig. 3D) and further supports our hypothesis. However, a trace of radioactivity was detected in the spinal region of cold compound injected mice. A possible explanation for this vague uptake is that the small portion of CXCR4 receptors are rapidly internalized and recycled to the cell surface,[44] which lead to the availability of new unoccupied receptors in the presence of competing compound.

4. Discussion

In this study, we sought to develop a novel small molecular CXCR4-targeted PET radioligand which is designed through a rational drug design approach not to change its authentic structure. Because our new tracer doesn't necessitate the additional labeling moieties such as chelators which can alter biological properties of the radioligand, we expect our PET tracer could be a more reliable noninvasive imaging probe to evaluate CXCR4-relavant diseases.

To achieve our goal, we determined the modifiable part of our CXCR4 antagonists[36] through highly predictive QSAR model, kernel-based partial least squares (KPLS) method with chemical fingerprint model (Canvas in Schrödinger Suite) (Fig. S1). At first, a series of our prior benzenesulfonamide compounds and their binding affinities to CXCR4 were analyzed by the KPLS/fingerprint model to access each atom's contribution to binding affinity (IC_{50}). This chemoinformatic model revealed each atom's impact on the predicted binding affinity and elucidated that the benzylamine group exerts a negative effect on affinity whereas the other part of compound makes a positive contribution to the affinity, suggesting that structural modification could be employed on this benzylamine moiety without affinity loss. Second, we designed a series of conceptualized radioligand structures by combining the positively contributing part of the scaffold with new components bearing fluorine atom in the modifiable part. Third, we estimated the affinity of each conceptualized structure to CXCR4 through molecular docking simulation (Glide in Schrödinger Suite), then screened out the compounds with high estimated affinity worthwhile to synthesize. In the molecular docking simulation, we tested two crystal structure of CXCR4 (3ODU and 3OE0), and used 3OE0 because it showed the better correlation with *in vitro* assay data of the known CXCR4-antagonists possessing benzenesulfonamide scaffold. 3ODU has higher resolution (2.5 Å) than 3OE0 (2.9 Å), but 3ODU is often unable to generate a consistent pose with X-ray structure and interactions with critical residues of CXCR4 as described in the previous literature.[33]

After synthesizing selected compounds (Scheme 1), we assessed actual biological activities of the compounds by two orthogonal in vitro assays such as receptor binding assay (Fig. S4) and chemotaxis inhibition assay (Fig. S5). Through these in vitro assays, we identified the compound **5** as the most potent one. In our binding assay, IC_{50} value of the compound **5** was determined to be 6.9 nM which is comparable to the affinity of reported prior antagonists (low nanomolar K_d).

Encouraged by the promising in vitro results, we conducted in vivo test using the compound **5** labeled with F-18 to evaluate the ability to visualize CXCR4-associated diseases such as inflammation, head and neck cancer, and metastatic lung cancer using the corresponding mouse models. Our mouse models exhibited preferential accumulation of tracers in the lesion of inflammation and orthotopic xenograft SCCHN, which are consistent with our anatomical studies (Fig 3). To explore the diagnostic potential of [^{18}F]**5** for cancer metastasis as well, we evaluated [^{18}F]**5** in our lung metastasis model and observed higher radioactivity accumulated in the sites of tumor growth, compared with the normal lung tissue area, and found modest tumor tissue wash-out over the course of a 90-min uptake period. Of note, the uptake of metabolic organs (liver: 1.20 ± 0.12 %ID/g and kidney: 3.22 ± 0.60 %ID/g) were relatively low, compared with prior CXCR4-tracers[21, 25, 45] likely due to the absence of the aforementioned cationic chelating moieties and faster clearance of the tracer.

While the present study provides an initial evaluation of [^{18}F]**5** as a PET imaging probe to visualize metastatic cancer guided along CXCR4 expression, the potential of this imaging probe to be served as an alternative to established PET agents such as FDG requires further

exploration. Wester *et al.* reported that CXCR4-targeted-cyclic peptide-conjugated chelate ([^{68}Ga]Pentixafor) displays more CXCR4-specific cancer images of multiple myeloma patients with higher contrast than FDG,[24] whereas the same tracer showed a lower radioactivity accumulation in solid tumors.[46] Hence, future studies should include comparing [^{18}F]**5** with established agents in a setting where we can evaluate our imaging probe's performance more rigorously using additional cancer models beyond our presented animal models.

5. Conclusion

In conclusion, we have described the synthesis, characterization, and biological evaluation of our novel PET-radiotracer, [^{18}F]**5**, as a CXCR4-specific imaging probe. The radiotracer was synthesized in high radiochemical yield and high radiochemical purity with stability in a biological buffer. Micro-PET imaging and biodistribution studies showed high accumulation in inflammatory lesion, human xenograft tumor, and metastatic lung tumor tissue of mice. Taken together, [^{18}F]**5** hold potential to serve as a CXCR4-specific imaging probe to diagnose and monitor the prognosis of inflammatory diseases, CXCR4-positive tumors, and metastatic cancers in the clinic.

Acknowledgements

The authors wish to thank Dr. Bryan Cox, Dr. Qi Shi and the late Dr. James P. Snyder for the help with computational modeling. We also thank Dr. Dennis C. Liotta for allowing us to use computation facilities.

Journal Pre-proofs

References

1. Tarasova, N. I.; Stauber, R. H.; Michejda, C. J., Spontaneous and Ligand-induced Trafficking of CXC-Chemokine Receptor 4. *J. Biol. Chem.* 1998, *273* (26), 15883-15886. doi:10.1074/jbc.273.26.15883.
2. Bleul, C. C.; Wu, L.; Hoxie, J. A.; Springer, T. A.; Mackay, C. R., The HIV coreceptors CXCR4 and CCR5 are differentially expressed and regulated on human T lymphocytes. *Proc. Natl. Acad. Sci. U. S. A.* 1997, *94* (5), 1925-1930. doi:10.1073/pnas.94.5.1925.
3. Oberlin, E.; Amara, A.; Bachelerie, F. o.; Bessia, C.; Virelizier, J.-L.; Arenzana-Seisdedos, F.; Schwartz, O.; Heard, J.-M.; Clark-Lewis, I.; Legler, D. F.; Loetscher, M.; Baggiolini, M.; Moser, B., The CXC chemokine SDF-1 is the ligand for LESTR/fusin and prevents infection by T-cell-line-adapted HIV-1. *Nature* 1996, *382*, 833-835. doi:10.1038/382833a0.
4. Kryczek, I.; Lange, A.; Mottram, P.; Alvarez, X.; Cheng, P.; Hogan, M.; Moons, L.; Wei, S.; Zou, L.; Machelon, V.; Emilie, D.; Terrassa, M.; Lackner, A.; Curiel, T. J.; Carmeliet, P.; Zou, W., CXCL12 and Vascular Endothelial Growth Factor Synergistically Induce Neoangiogenesis in Human Ovarian Cancers. *Cancer Res.* 2005, *65* (2), 465-472.
5. Murdoch; Monk; Finn, Functional expression of chemokine receptor CXCR4 on human epithelial cells. *Immunology* 1999, *98* (1), 36-41. doi:doi:10.1046/j.1365-2567.1999.00848.x.
6. Weitzenfeld, P.; Ben-Baruch, A., The chemokine system, and its CCR5 and CXCR4 receptors, as potential targets for personalized therapy in cancer. *Cancer Lett.* 2014, *352* (1), 36-53. doi:10.1016/j.canlet.2013.10.006.
7. Sun, S. H., Roles of P2X7 receptor in glial and neuroblastoma cells: the therapeutic potential of P2X7 receptor antagonists. *Mol. Neurobiol.* 2010, *41* (2-3), 351-5. doi:10.1007/s12035-010-8120-x.
8. Zlotnik, A.; Burkhardt, A. M.; Homey, B., Homeostatic chemokine receptors and organ-specific metastasis. *Nat. Rev. Immunol.* 2011, *11* (9), 597-606. doi:10.1038/nri3049.
9. Raman, D.; Sobolik-Delmaire, T.; Richmond, A., Chemokines in health and disease. *Exp. Cell Res.* 2011, *317* (5), 575-589. doi:https://doi.org/10.1016/j.yexcr.2011.01.005.
10. Balkwill, F. R., The chemokine system and cancer. *J. Pathol.* 2012, *226* (2), 148-157. doi:doi:10.1002/path.3029.
11. Debnath, B.; Xu, S.; Grande, F.; Garofalo, A.; Neamati, N., Small Molecule Inhibitors of CXCR4. *Theranostics* 2013, *3* (1), 47-75. doi:10.7150/thno.5376.
12. Grande, F.; Giancotti, G.; Ioele, G.; Occhiuzzi, M. A.; Garofalo, A., An update on small molecules targeting CXCR4 as starting points for the development of anti-cancer therapeutics. *Eur. J. Med. Chem.* 2017, *139*, 519-530. doi:10.1016/j.ejmech.2017.08.027.
13. Choi, W.-T.; Duggineni, S.; Xu, Y.; Huang, Z.; An, J., Drug Discovery Research Targeting the CXC Chemokine Receptor 4 (CXCR4). *J. Med. Chem.* 2012, *55* (3), 977-994. doi:10.1021/jm200568c.
14. George, G. P. C.; Pisaneschi, F.; Nguyen, Q.-D.; Aboagye, E. O., Positron Emission Tomographic Imaging of CXCR4 in Cancer: Challenges and Promises. *Mol. Imaging* 2014, *13*, 1-19. doi:10.2310/7290.2014.00041.
15. Kuil, J.; Buckle, T.; van Leeuwen, F. W. B., Imaging agents for the chemokine receptor 4 (CXCR4). *Chem. Soc. Rev.* 2012, *41* (15), 5239-5261. doi:10.1039/C2CS35085H.
16. Tamamura, H.; Xu, Y.; Hattori, T.; Zhang, X.; Arakaki, R.; Kanbara, K.; Omagari, A.; Otaka, A.; Ibuka, T.; Yamamoto, N., A low-molecular-weight inhibitor against the

chemokine receptor CXCR4: a strong anti-HIV peptide T140. *Biochem. Biophys. Res. Commun.* 1998, *253* (3), 877-882.

17. Fujii, N.; Oishi, S.; Hiramatsu, K.; Araki, T.; Ueda, S.; Tamamura, H.; Otaka, A.; Kusano, S.; Terakubo, S.; Nakashima, H., Molecular-size reduction of a potent CXCR4-chemokine antagonist using orthogonal combination of conformation-and sequence-based libraries. *Angew. Chem. Int. Ed. Engl.* 2003, *42* (28), 3251-3253.
18. Schols, D.; Struyf, S.; Van Damme, J.; Esté, J. A.; Henson, G.; De Clercq, E., Inhibition of T-tropic HIV strains by selective antagonization of the chemokine receptor CXCR4. *J. Exp. Med.* 1997, *186* (8), 1383-1388.
19. Gourni, E.; Demmer, O.; Schottelius, M.; D'Alessandria, C.; Schulz, S.; Dijkgraaf, I.; Schumacher, U.; Schwaiger, M.; Kessler, H.; Wester, H.-J., PET of CXCR4 Expression by a 68Ga-Labeled Highly Specific Targeted Contrast Agent. *J. Nucl. Med.* 2011, *52* (11), 1803-1810. doi:10.2967/jnumed.111.098798.
20. Hennrich, U.; Seyler, L.; Schäfer, M.; Bauder-Wüst, U.; Eisenhut, M.; Semmler, W.; Bäuerle, T., Synthesis and in vitro evaluation of 68Ga-DOTA-4-FBn-TN14003, a novel tracer for the imaging of CXCR4 expression. *Bioorg. Med. Chem.* 2012, *20* (4), 1502-1510. doi:https://doi.org/10.1016/j.bmc.2011.12.052.
21. Jacobson, O.; Weiss, I. D.; Szajek, L. P.; Niu, G.; Ma, Y.; Kiesewetter, D. O.; Peled, A.; Eden, H. S.; Farber, J. M.; Chen, X., Improvement of CXCR4 tracer specificity for PET imaging. *J. Control. Release* 2012, *157* (2), 216-223. doi:https://doi.org/10.1016/j.jconrel.2011.09.076.
22. Nimmagadda, S.; Pullambhatla, M.; Stone, K.; Green, G.; Bhujwalla, Z. M.; Pomper, M. G., Molecular Imaging of CXCR4 Receptor Expression in Human Cancer Xenografts with [^{64}Cu]AMD3100 Positron Emission Tomography. *Cancer Res.* 2010, *70* (10), 3935-3944. doi:10.1158/0008-5472.can-09-4396.
23. De Silva, R. A.; Peyre, K.; Pullambhatla, M.; Fox, J. J.; Pomper, M. G.; Nimmagadda, S., Imaging CXCR4 Expression in Human Cancer Xenografts: Evaluation of Monocyclam 64Cu-AMD3465. *J. Nucl. Med.* 2011, *52* (6), 986-993. doi:10.2967/jnumed.110.085613.
24. Wester, H. J.; Keller, U.; Schottelius, M.; Beer, A.; Philipp-Abbrederis, K.; Hoffmann, F.; Šimeček, J.; Gerngross, C.; Lassmann, M.; Herrmann, K.; Pellegata, N.; Rudelius, M.; Kessler, H.; Schwaiger, M., Disclosing the CXCR4 Expression in Lymphoproliferative Diseases by Targeted Molecular Imaging. *Theranostics* 2015, *5* (6), 618-630. doi:10.7150/thno.11251.
25. Poschenrieder, A.; Schottelius, M.; Schwaiger, M.; Wester, H. J., Preclinical evaluation of [(68)Ga]NOTA-pentixafor for PET imaging of CXCR4 expression in vivo - a comparison to [(68)Ga]pentixafor. *EJNMMI Res* 2016, *6:70* (1), 1-5. doi:10.1186/s13550-016-0227-2.
26. Amor-Coarasa, A.; Kelly, J. M.; Singh, P. K.; Ponnala, S.; Nikolopoulou, A.; Williams, C., Jr.; Vedvyas, Y.; Jin, M. M.; Warren, J. D.; Babich, J. W., [(18)F]Fluoroethyltriazolyl Monocyclam Derivatives as Imaging Probes for the Chemokine Receptor CXCR4. *Molecules (Basel, Switzerland)* 2019, *24* (8), 1612. doi:10.3390/molecules24081612.
27. Zhang, X.-X.; Sun, Z.; Guo, J.; Wang, Z.; Wu, C.; Niu, G.; Ma, Y.; Kiesewetter, D. O.; Chen, X., Comparison of 18F-labeled CXCR4 antagonist peptides for PET imaging

of CXCR4 expression. *Mol. Imaging Biol.* 2013, *15* (6), 758-767. doi:10.1007/s11307-013-0640-0.

28. Jacobson, O.; Weiss, I. D.; Kiesewetter, D. O.; Farber, J. M.; Chen, X., PET of Tumor CXCR4 Expression with 4-18F-T140. *J. Nucl. Med.* 2010, *51* (11), 1796-1804. doi:10.2967/jnumed.110.079418.
29. Amor-Coarasa, A.; Kelly, J.; Ponnala, S.; Vedvyas, Y.; Nikolopoulou, A.; Williams, C., Jr.; Jin, M. M.; David Warren, J.; Babich, J. W., [(18)F]RPS-544: A PET tracer for imaging the chemokine receptor CXCR4. *Nucl. Med. Biol.* 2018, *60*, 37-44. doi:10.1016/j.nucmedbio.2018.01.004.
30. Brickute, D.; Braga, M.; Kaliszczak, M. A.; Barnes, C.; Lau, D.; Carroll, L.; Stevens, E.; Trousil, S.; Alam, I. S.; Nguyen, Q.-D.; Aboagye, E. O., Development and Evaluation of an (18)F-Radiolabeled Monocyclam Derivative for Imaging CXCR4 Expression. *Mol. Pharm.* 2019, *16* (5), 2106-2117. doi:10.1021/acs.molpharmaceut.9b00069.
31. Jacobson, O.; Weiss, I. D.; Szajek, L.; Farber, J. M.; Kiesewetter, D. O., 64Cu-AMD3100—a novel imaging agent for targeting chemokine receptor CXCR4. *Bioorg. Med. Chem.* 2009, *17* (4), 1486-1493.
32. Woodard, L. E.; De Silva, R. A.; Azad, B. B.; Lisok, A.; Pullambhatla, M.; Lesniak, W. G.; Mease, R. C.; Pomper, M. G.; Nimmagadda, S., Bridged cyclams as imaging agents for chemokine receptor 4 (CXCR4). *Nucl. Med. Biol.* 2014, *41* (7), 552-561.
33. Cox, B. D.; Prosser, A. R.; Katzman, B. M.; Alcaraz, A. A.; Liotta, D. C.; Wilson, L. J.; Snyder, J. P., Anti-HIV Small-Molecule Binding in the Peptide Subpocket of the CXCR4: CVX15 Crystal Structure. *Chembiochem* 2014, *15* (11), 1614-1620.
34. Sirion, U.; Kim, H. J.; Lee, J. H.; Seo, J. W.; Lee, B. S.; Lee, S. J.; Oh, S. J.; Chi, D. Y., An efficient F-18 labeling method for PET study: Huisgen 1, 3-dipolar cycloaddition of bioactive substances and F-18-labeled compounds. *Tetrahedron Lett.* 2007, *48* (23), 3953-3957.
35. Yoon, Y.; Liang, Z.; Zhang, X.; Choe, M.; Zhu, A.; Cho, H. T.; Shin, D. M.; Goodman, M. M.; Chen, Z.; Shim, H., CXC Chemokine Receptor-4 Antagonist Blocks Both Growth of Primary Tumor and Metastasis of Head and Neck Cancer in Xenograft Mouse Models. *Cancer Res.* 2007, *67* (15), 7518-7524. doi:10.1158/0008-5472.can-06-2263.
36. Mooring, S. R.; Liu, J.; Liang, Z.; Ahn, J.; Hong, S.; Yoon, Y.; Snyder, J. P.; Shim, H., Benzenesulfonamides: A Unique Class of Chemokine Receptor Type 4 Inhibitors. *ChemMedChem* 2013, *8* (4), 622-632. doi:10.1002/cmdc.201200582.
37. Wu, B.; Chien, E. Y.; Mol, C. D.; Fenalti, G.; Liu, W.; Katritch, V.; Abagyan, R.; Brooun, A.; Wells, P.; Bi, F. C., Structures of the CXCR4 chemokine GPCR with small-molecule and cyclic peptide antagonists. *Science* 2010, *330* (6007), 1066-1071.
38. Banerjee, A.; Maschauer, S.; Hübner, H.; Gmeiner, P.; Prante, O., Click chemistry based synthesis of dopamine D4 selective receptor ligands for the selection of potential PET tracers. *Bioorg. Med. Chem. Lett.* 2013, *23* (22), 6079-6082.
39. Liang, Z.; Zhan, W.; Zhu, A.; Yoon, Y.; Lin, S.; Sasaki, M.; Klapproth, J.-M. A.; Yang, H.; Grossniklaus, H. E.; Xu, J.; Rojas, M.; Voll, R. J.; Goodman, M. M.; Arrendale, R. F.; Liu, J.; Yun, C. C.; Snyder, J. P.; Liotta, D. C.; Shim, H., Development of a Unique Small Molecule Modulator of CXCR4. *PLoS One* 2012, *7* (4), e34038. doi:10.1371/journal.pone.0034038.

40. Lu, D. Y.; Tang, C. H.; Yeh, W. L.; Wong, K. L.; Lin, C. P.; Chen, Y. H.; Lai, C. H.; Chen, Y. F.; Leung, Y. M.; Fu, W. M., SDF-1alpha up-regulates interleukin-6 through CXCR4, PI3K/Akt, ERK, and NF-kappaB-dependent pathway in microglia. *Eur. J. Pharmacol.* 2009, *613* (1-3), 146-54. doi:10.1016/j.ejphar.2009.03.001.
41. Chung, S.-H.; Seki, K.; Choi, B.-I.; Kimura, K. B.; Ito, A.; Fujikado, N.; Saijo, S.; Iwakura, Y., CXC chemokine receptor 4 expressed in T cells plays an important role in the development of collagen-induced arthritis. *Arthritis Res. Ther.* 2010, *12* (5), R188.
42. Werner, L.; Guzner-Gur, H.; Dotan, I., Involvement of CXCR4/CXCR7/CXCL12 Interactions in Inflammatory bowel disease. *Theranostics* 2013, *3* (1), 40.
43. Wang, A.; Guilpain, P.; Chong, B. F.; Chouzenoux, S.; Guillevin, L.; Du, Y.; Zhou, X. J.; Lin, F.; Fairhurst, A. M.; Boudreaux, C., Dysregulated expression of CXCR4/CXCL12 in subsets of patients with systemic lupus erythematosus. *Arthritis Rheum.* 2010, *62* (11), 3436-3446.
44. Förster, R.; Kremmer, E.; Schubel, A.; Breitfeld, D.; Kleinschmidt, A.; Nerl, C.; Bernhardt, G.; Lipp, M., Intracellular and Surface Expression of the HIV-1 Coreceptor CXCR4/Fusin on Various Leukocyte Subsets: Rapid Internalization and Recycling Upon Activation. *J. Immunol.* 1998, *160* (3), 1522-1531.
45. Yu, X.; Huang, Y.; Collin-Osdoby, P.; Osdoby, P., Stromal cell-derived factor-1 (SDF-1) recruits osteoclast precursors by inducing chemotaxis, matrix metalloproteinase-9 (MMP-9) activity, and collagen transmigration. *J. Bone Miner. Res.* 2003, *18* (8), 1404-18. doi:10.1359/jbmr.2003.18.8.1404.
46. Vag, T.; Gerngross, C.; Herhaus, P.; Eiber, M.; Philipp-Abbrederis, K.; Graner, F.-P.; Ettl, J.; Keller, U.; Wester, H.-J.; Schwaiger, M., First Experience with Chemokine Receptor CXCR4–Targeted PET Imaging of Patients with Solid Cancers. *J. Nucl. Med.* 2016, *57* (5), 741-746. doi:10.2967/jnumed.115.161034.

Journal Pre-proofs

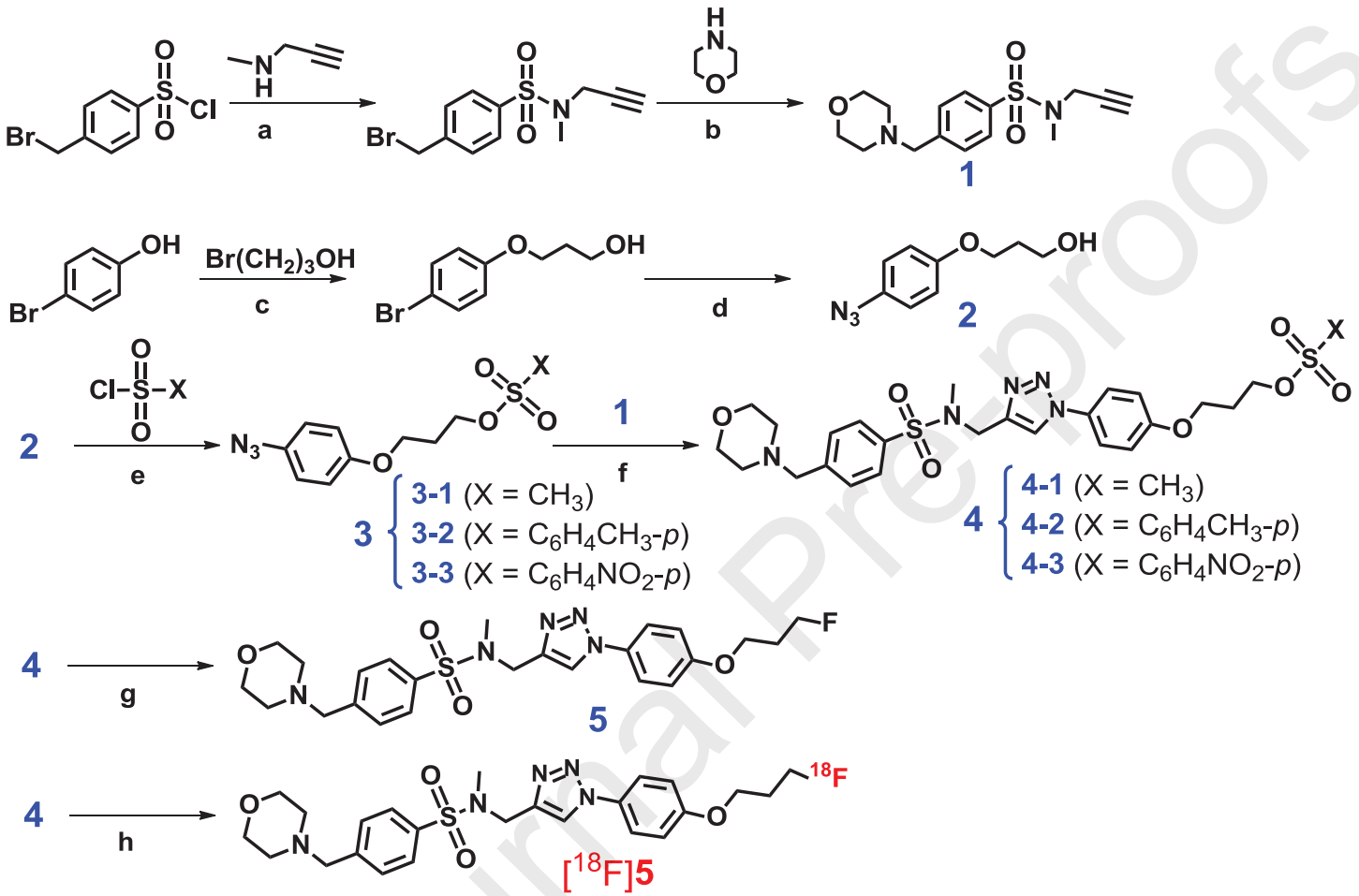

Scheme 1. Reagents and conditions: (a) DCM, TEA, ice bath to r. t., 6 h, 75%; (b) MeCN, r.t., 12 h, 75%; (c) DMF, K_2CO_3, 70 °C, 51%; (d) DMF, NaN_3, CuI, DMEDA, EtOH/H_2O (7:3), 80 °C, 6 h, 80%; (e) DCM, TEA, DMAP, 0 °C, 30 min; 70%, X = CH_3 or $C_6H_4CH_3$-*p* or $C_6H_4NO_2$-*p*; (f) THF/H_2O (10:1), $CuSO_4$, sodium ascorbate, r.t., 3 h, 60%; (g) *t*-BuOH, CsF, reflux, 3 h, 51%; (h) MeCN, K_2CO_3, K_{222}, $[^{18}F]F^-$

Journal Pre-proofs

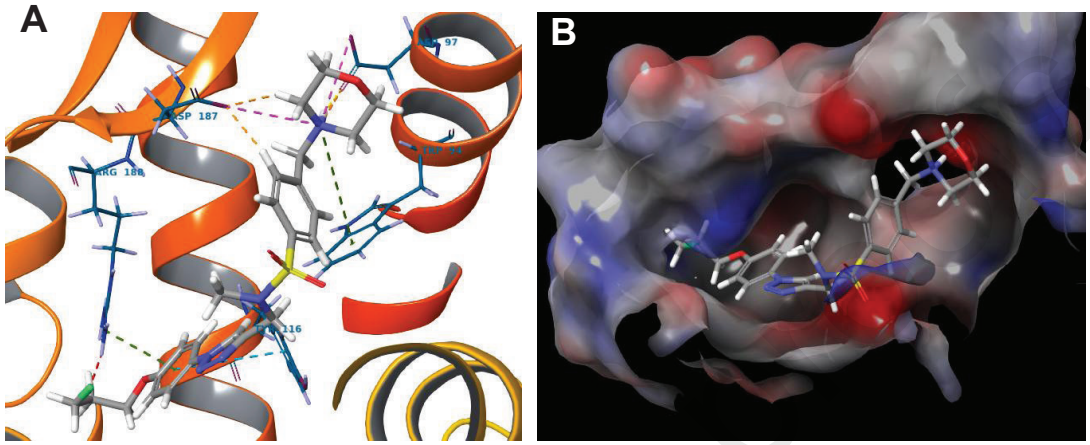

Figure 1. **Docking pose of Compound 5 in the CXCR4 crystal structure** (A) Docking pose representing the interactions of compound 5 with the critical residues of CXCR4 (W94, D97, Y116, D187, R188). Dotted lines show putative hydrogen bonds. (B) Molecular surface representation of the binding pocket of CXCR4 receptor in the crystal structure [PDB ID: 3OE0] colored by atom type (carbon and hydrogen: light grey; nitrogen: blue; oxygen: red). The ligand (Compound **5**) is represented by stick models.

Journal Pre-proof

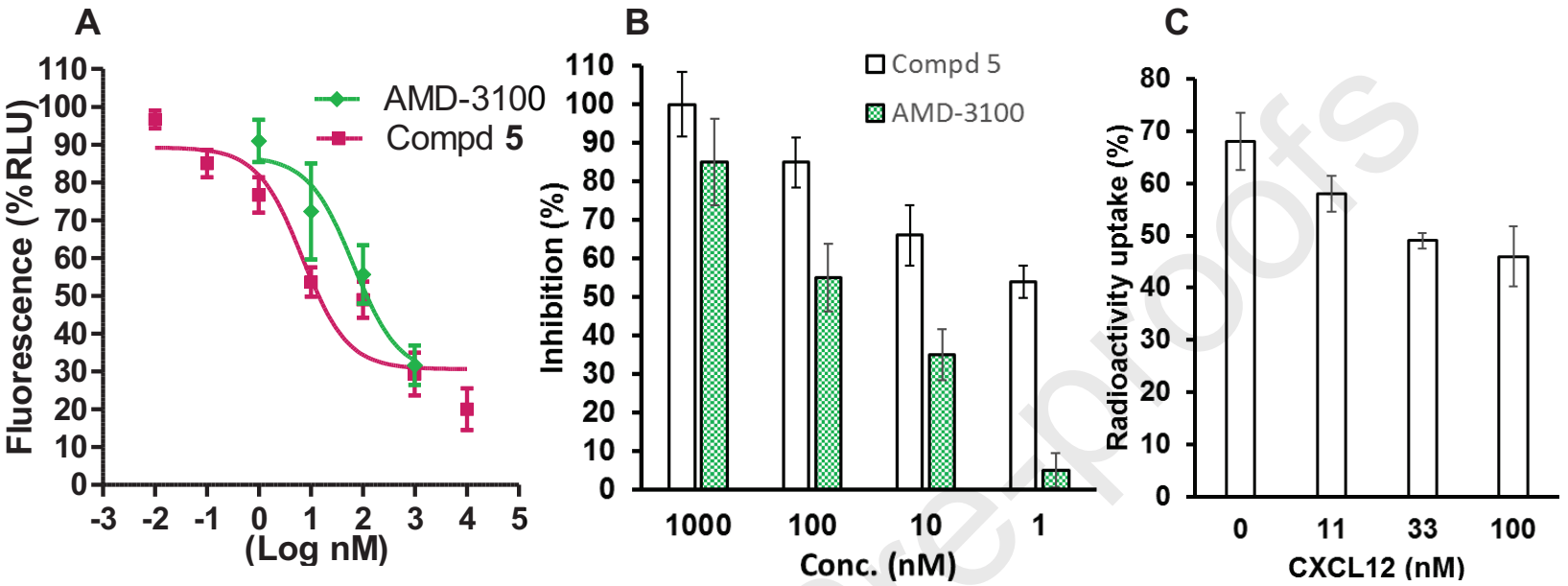

Figure 2. In vitro assays of compound 5 (A) Competition-binding assay using the biotinylated CXCR4 antagonist TN14003. MDA-MB-231 cells on an 8-well slide chamber were treated with various concentrations of compound 5 and biotin-labeled TN14003. After washing, cells were incubated with streptavidin-rhodamine. Mean fluorescence intensity was quantitated with ImageJ (triplicate). (B) Matrigel invasion assay induced by CXCR4/CXCL12-mediated chemotaxis using MDA-MB-231 cells in the presence of compound 5. The invasion % was determined by counting the H&E-stained cells (triplicate). (C) In vitro cellular uptake assay with hot compound [18F]5 and CXCL12 as a competitive ligand. CXCR4-positive metastatic squamous cell carcinoma of head and neck (SCCHN) cells were preincubated with radiolabeled ligand and natural ligand (CXCL12) were added to make final concentrations of 11, 33, and 100 nM. After 60 min incubation and washing, radioactivity of each tube was measured by a gamma counter (triplicate). Error bars indicate standard deviations.

Journal Pre-proofs

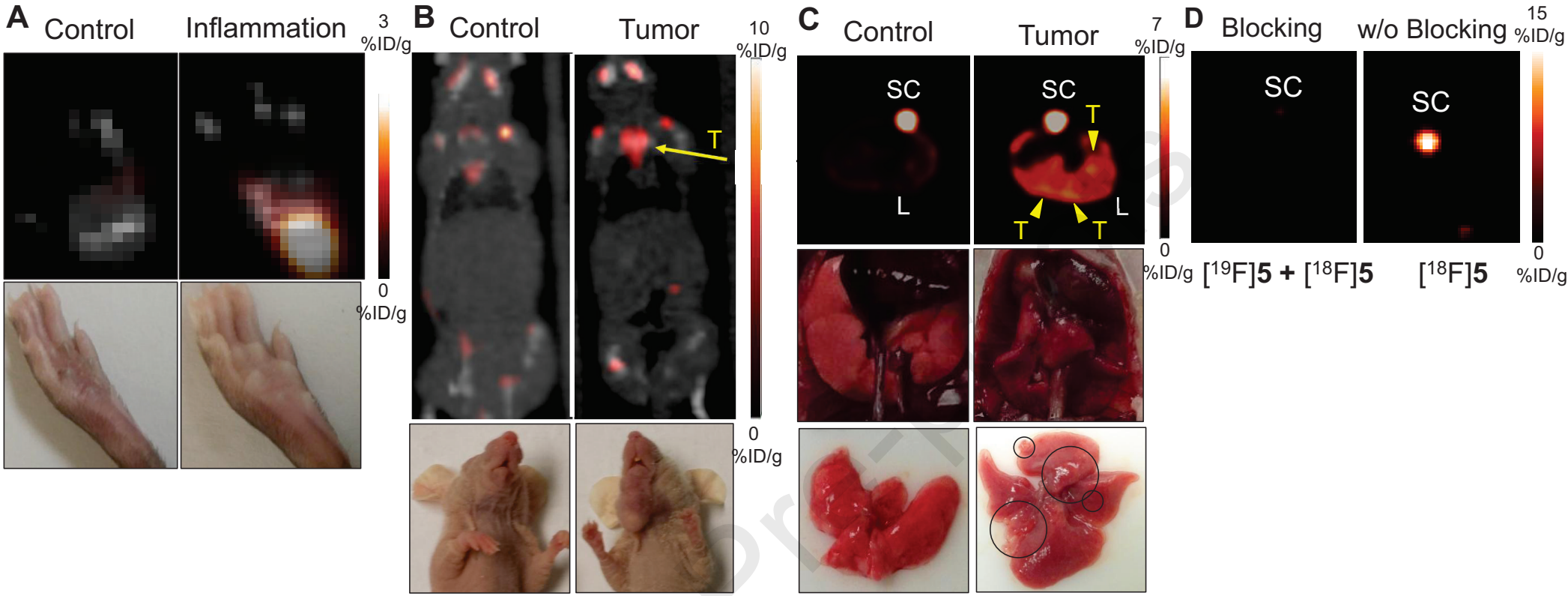

Figure 3. μPET/CT images of [^{18}F]5 (A) Acute inflammation was induced by subcutaneous injection of λ-carrageenan into one of the hind paws of male nude mice. An apparent edema response was observed 5 h after the λ-carrageenan injection. Radiotracer ([^{18}F]**5**) was injected to mice through the tail vein. Then, mice were anaesthetized with isoflurane. 70 min after injection of radiotracer, PET images were acquired for 20 min using an Inveon micro PET/CT Preclinical Scanner (Siemens). Subsequent CT images were acquired for 10 min. (B) SCCHN (squamous cell carcinoma of head and neck) CXCR4-positive tumor cells were inoculated (2.5×10^6 cells in 50 μL) to female nude mouse in the area of neck (orthotopic), 3 weeks before in vivo test. PET/CT images were acquired using the same protocol as the paw edema case. Tumor (T) is indicated by yellow arrows. (C) Six-week-old female nude mice were given injections of 2.0×10^6 metastatic subclones of E3 (CXCR4-positive murine carcinoma cell line) through the tail vein. After 8 weeks, PET/CT images were acquired using the same protocol as the SCCHN cancer study. Representative [^{18}F]**5** transverse PET images of 90 min p.i., Yellow arrows and text denote the location of the tumor (T), lung (L), spinal column (SC). The circles in the bottom figure indicate induced metastatic tumor nodules. (D) μPET transverse plane images with cold + hot (Blocking, left) compd. vs only hot compd. (right); For the blocking, 200 μL of cold [^{19}F]**5** solution (30 mg/kg, 10% DMSO, 90% PBS including 45% cyclodextrin) was administered to the mouse (i.p.) (male, 6 weeks, 20 g, Jackson Laboratory, Strain JAZ 007850 J:NU) 30 min prior to [^{18}F]**5** injection (i.v.). PET images were acquired using the same protocol as the paw edema case. This experiment suggests the specificity of compound **5** to bind CXCR4-positive stem cells in bone marrow.

Journal Pre-proof

Table 1. Biodistribution of [^{18}F]**5** at 90 min

Organ	SUV (%ID/g)	*P* (n = 5)
Paw edema	1.53 ± 0.08	0.002
SCCHN tumor	4.00 ± 0.28	0.005
Metastatic tumor in lung	1.66 ± 0.14	0.002
Lung	0.50 ± 0.04	n/a
Liver	1.20 ± 0.12	n/a
Kidney	3.22 ± 0.60	n/a
Muscle	0.16 ± 0.03	n/a
Heart	0.54 ± 0.08	n/a
Spleen	0.58 ± 0.07	n/a
Small intestine	0.68 ± 0.04	n/a
Large intestine	0.17 ± 0.04	n/a

Journal Pre-proofs

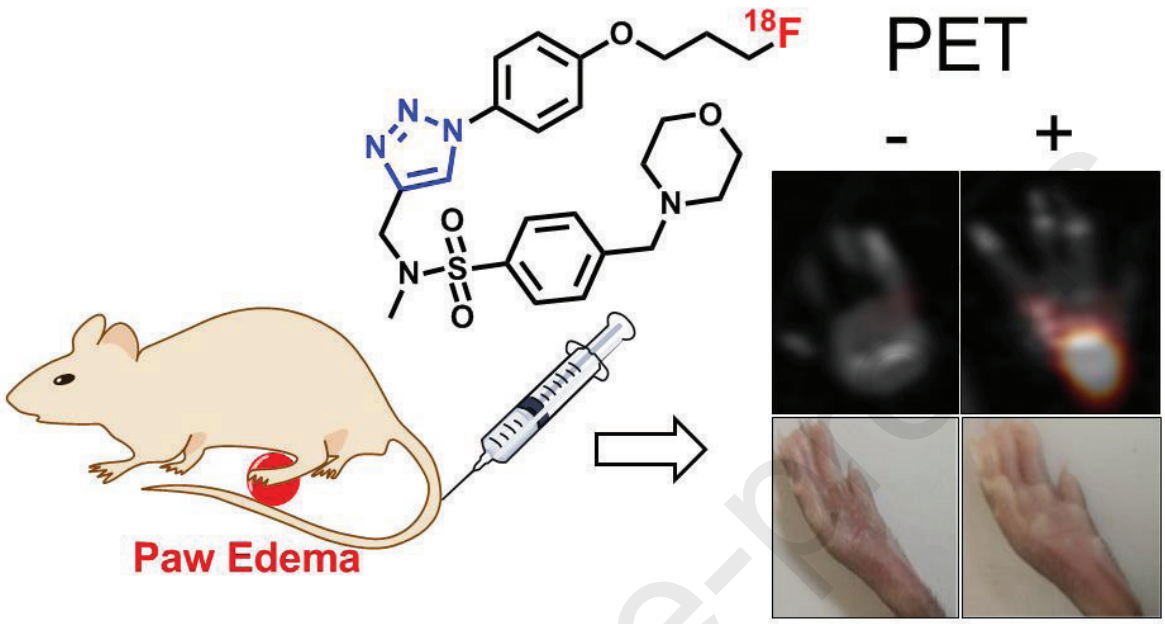

Journal Pre-proofs

Scheme 1. Reagents and conditions: (a) DCM, TEA, ice bath to r. t., 6 h, 75%; (b) MeCN, r.t., 12 h, 75%; (c) DMF, K_2CO_3, 70 °C, 51%; (d) DMF, NaN_3, CuI, DMEDA, EtOH/H_2O (7:3), 80 °C, 6 h, 80%; (e) DCM, TEA, DMAP, 0 °C, 30 min; 70%, X = CH_3 or $C_6H_4CH_3$-*p* or $C_6H_4NO_2$-*p*; (f) THF/H_2O (10:1), $CuSO_4$, sodium ascorbate, r.t., 3 h, 60%; (g) *t*-BuOH, CsF, reflux, 3 h, 51%; (h) MeCN, K_2CO_3, K_{222}, [^{18}F]F^-

Figure 1. **Docking pose of Compound 5 in the CXCR4 crystal structure** (A) Docking pose representing the interactions of compound 5 with the critical residues of CXCR4 (W94, D97, Y116, D187, R188). Dotted lines show putative hydrogen bonds. (B) Molecular surface representation of the binding pocket of CXCR4 receptor in the crystal structure [PDB ID: 3OE0] colored by atom type (carbon and hydrogen: light grey; nitrogen: blue; oxygen: red). The ligand (Compound **5**) is represented by stick models.

Figure 2. In vitro assays of compound 5 (A) Competition-binding assay using the biotinylated CXCR4 antagonist TN14003. MDA-MB-231 cells on an 8-well slide chamber were treated with various concentrations of compound 5 and biotin-labeled TN14003. After washing, cells were incubated with streptavidin-rhodamine. Mean fluorescence intensity was quantitated with ImageJ (triplicate). (B) Matrigel invasion assay induced by CXCR4/CXCL12-mediated chemotaxis using MDA-MB-231 cells in the presence of compound 5. The invasion % was determined by counting the H&E-stained cells (triplicate). (C) In vitro cellular uptake assay with hot compound [18F]5 and CXCL12 as a competitive ligand. CXCR4-positive metastatic squamous cell carcinoma of head and neck (SCCHN) cells were preincubated with radiolabeled ligand and natural ligand (CXCL12) were added to make final concentrations of 11, 33, and 100 nM. After 60 min incubation and washing, radioactivity of each tube was measured by a gamma counter (triplicate). Error bars indicate standard deviations.

Figure 3. μPET/CT images of [^{18}F]5 (A) Acute inflammation was induced by subcutaneous injection of λ-carrageenan into one of the hind paws of male nude mice. An apparent edema response was observed 5 h after the λ-carrageenan injection. Radiotracer ([^{18}F]**5**) was injected to mice through the tail vein. Then, mice were anaesthetized with isoflurane. 70 min after injection of radiotracer, PET images were acquired for 20 min using an Inveon micro PET/CT Preclinical Scanner (Siemens). Subsequent CT images were acquired for 10 min. (B) SCCHN (squamous cell carcinoma of head and neck) CXCR4-positive tumor cells were inoculated (2.5×10^6 cells in 50 μL) to female nude mouse in the area of neck (orthotopic), 3 weeks before in vivo test. PET/CT images were acquired using the same protocol as the paw edema case. Tumor (T) is indicated by yellow arrows. (C) Six-week-old female nude mice were given injections of 2.0×10^6 metastatic subclones of E3 (CXCR4-positive murine carcinoma cell line) through the tail vein. After 8 weeks, PET/CT images were acquired using the same protocol as the SCCHN cancer study. Representative [^{18}F]**5** transverse PET images of 90 min p.i., Yellow arrows and text denote the location of the tumor (T), lung (L), spinal column (SC). The circles in the bottom figure indicate induced metastatic tumor nodules. (D) μPET transverse plane images with cold + hot (Blocking, left) compd. vs only hot compd. (right); For the blocking, 200 μL of cold [^{19}F]**5** solution (30 mg/kg, 10% DMSO,

90% PBS including 45% cyclodextrin) was administered to the mouse (i.p.) (male, 6 weeks, 20 g, Jackson Laboratory, Strain JAZ 007850 J:NU) 30 min prior to [^{18}F]**5** injection (i.v.). PET images were acquired using the same protocol as the paw edema case. This experiment suggests the specificity of compound **5** to bind CXCR4-positive stem cells in bone marrow.

Table 1. Biodistribution of [^{18}F]**5** at 90 min

Organ	SUV (%ID/g)	*P* (n = 5)
Paw edema	1.53 ± 0.08	0.002
SCCHN tumor	4.00 ± 0.28	0.005
Metastatic tumor in lung	1.66 ± 0.14	0.002
Lung	0.50 ± 0.04	n/a
Liver	1.20 ± 0.12	n/a
Kidney	3.22 ± 0.60	n/a
Muscle	0.16 ± 0.03	n/a
Heart	0.54 ± 0.08	n/a
Spleen	0.58 ± 0.07	n/a
Small intestine	0.68 ± 0.04	n/a
Large intestine	0.17 ± 0.04	n/a

Journal Pre-proofs

Declaration of interests

☒ The authors declare that they have no known competing financial interests or personal relationships that could have appeared to influence the work reported in this paper.

☐The authors declare the following financial interests/personal relationships which may be considered as potential competing interests:

Journal Pre-proofs